Thermal Regeneration of Diesel-Particulate Monolithic Filters

A mathematical model is developed to describe the process of thermal regeneration in diesel-particulate monolithic filters. The model shows that a typical regeneration cycle consists of four stages: preheating, ignition, transport-controlled combustion, and cooling. The total regeneration time and the peak temperature are the important regeneration characteristics and can be controlled by initial particulate loading, total filtration area, and channel wall thickness.

E. J. BISSETT

Mathematics Department
General Motors Research Laboratories
Warren, MI 48090

FARHANG SHADMAN

Department of Chemical Engineering
University of Arizona
Tucson, AZ 85721

SCOPE

Various types of filters are being considered for the removal of particulates from diesel exhaust. The idea of a filter consisting of either a fibrous or a porous ceramic medium which can be regenerated on board has received much attention. Thermal regeneration is an intermittent process during which some auxiliary heat is supplied to the filter to burn out the collected particles. The process is complex and if not properly controlled can be either too slow with little regeneration, or too fast with the risk of damage to the filter because of high temperature peaks. Considering the type of application, a very reliable and reproducible process is required which can occur many times with no operator's attention. Therefore, a good understanding of the process and a systematic parametric study is necessary. In an earlier work (Shadman and Bissett, 1983), a theoretical model for the regeneration of fibrous filters was developed which succeeded in clarifying some of the subtle features of the process. However, wall-flow monolithic filters are surface filters and do not necessarily have the same regeneration characteristics as fibrous filters, which are depth filters. The objective of this study is to develop a model for the regeneration of monolithic filters which can help in understanding the process and can facilitate parametric study and design optimization.

CONCLUSIONS AND SIGNIFICANCE

Unlike the case of fibrous filters, the spatial temperature distribution in monolithic filters is nearly uniform for typical exhaust flow rates and varies only with time. The regeneration process consists of four stages: a preheating stage during which the filter is heated by the exhaust gas, an ignition stage in which significant reaction begins in the deposit and the temperature increases steeply, a transport-controlled stage in which most of the deposit burns but at a rate limited by the availability of oxygen, and finally a cooling stage during which the accumulated heat of combustion gradually dissipates. Among the various design variables, the initial particulate loading, the filtration area, and the channel wall thickness are particularly important. An increase in particulate loading and/or a decrease in filtration area or wall thickness improves the rate of regeneration but results in a larger temperature peak and a higher risk of damage to the filter. However, the model shows that acceptable regeneration with reasonable values for parameters is possible. The model can be further used as part of an optimization scheme to find the best design.

INTRODUCTION

In an effort to reduce particulate emissions from diesel-powered vehicles, various exhaust filtration systems are currently under consideration. All such systems must face the problem of disposing of the particulates collected from the exhaust stream and deposited in the filter system, regardless of the precise manner of collection. One solution to this problem is thermal regeneration, in which heat is added to the system in such a way as to burn the deposited particulates. This added heat is usually supplied to the exhaust gas either by an auxiliary heat source such as a burner, or by throttling the intake air to the engine. The auxiliary heat may be applied either continuously in time or intermittently; intake air throttling is only performed intermittently so that the engine performance, averaged over a complete collection/regeneration cycle, is only minimally affected. This report will focus on the more dynamically complex thermal regenerations associated with intermittent operation, for example those resulting from intake air throttling, although the case of an auxiliary heat source can be studied in precisely the same manner.

In a previous paper (Shadman and Bissett, 1983), the authors presented an analytical model of the combustion process in a fi-

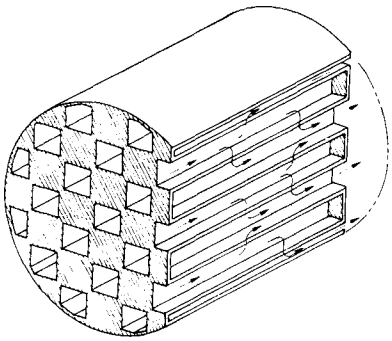

Figure 1. Schematic view of a wall-flow monolith filter.

brous filter system during throttle-initiated thermal regeneration. In the current paper, the principal purpose is to perform a similar analysis for a wall-flow monolith filter. The mechanisms of both collection and regeneration in monolithic filters are different from those in fibrous filters. In monolith filters the convective flow of gas is through the porous deposited layer of particles, while in fibrous filters the convective flow is over the deposited particulate layer. This is responsible for the very high filtration efficiency of monoliths. It also results in a different regeneration mechanism. Experiments show that monolithic filters are difficult to regenerate and require more heat than is normally available using intake air throttling.

The regeneration of monolithic filters has some similarities with the regeneration of coked, fixed-bed reactors, a process which has been analyzed and modeled extensively, for example by Johnson et al. (1962), Olson et al. (1968), and Rhee et al. (1973, 1974). However, the existing models cannot be applied to this case because of certain basic differences in geometry and in the physical characteristics of the bed. These differences will be noted in subsequent sections. Therefore, an analysis of the regeneration in monolithic filters is required to understand the nature of the process and to evaluate the potential of such filters as a possible particulate removal system.

MODEL FORMULATION

A wall-flow monolith, schematically shown in Figure 1, is made from a high-temperature ceramic material by extrusion. Plugging adjacent channels alternately at opposite ends forces the exhaust stream through the porous ceramic walls as shown in Figure 1. Solid particulates in the exhaust gas stream are trapped on the upstream sides of the channel walls typically with greater than 90% efficiency. Figure 2 is a typical micrograph of a section of loaded monolith and shows that the particulates deposit as a layer on the upstream side of the channel walls with little penetration into the interior pores of the monolith.

The idealization of this physical system that will provide the basis for the modeling described here is shown in Figure 3. The gas flows through two layers: the first is the particle deposit, which shrinks with time during regeneration; the second layer is the porous channel wall, which remains unchanged. Some change in the internal structure of the deposit during reaction is expected. However, these changes have not been studied and cannot be characterized accurately at this stage. Therefore they will be neglected, and only the thickness of the deposit layer will vary with time. Although the model allows reaction throughout the deposit layer, model results presented later show that the regeneration itself causes most particle depletion to occur in a thin layer near the particle layer surface. This depletion mode is consistent with our simplifying assumption that the reaction consumes the deposit by shrinking its thickness without changing its internal structure. Because the duration of regeneration is short, the addition of particles to the deposit during regeneration can be neglected. The described bed geometry, and particularly the change in bed depth with time, is an example of the unique features which make this

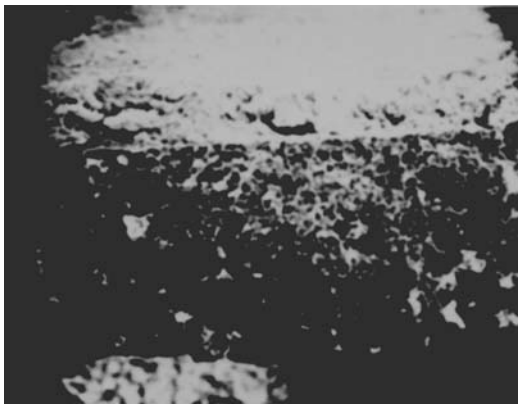

Figure 2. Scanning electron micrograph of the fractured edge of a loaded wall-flow monolith (magnification: 62 X); fracture made longitudinally down the channel.

system different from other fixed-bed reactors.

Only a single spatial variable, x in Figure 3, will be used in this modeling, and all variations in the direction perpendicular to x will be neglected. Since the combined flow resistance of the porous ceramic walls and the particle deposit is much greater than the flow resistance of the open monolith channels, the flow distributes itself uniformly over the entire filtration area of a loaded wall-flow monolith filter. Such a uniform flow pattern should uniformly load the filtration area with particles since such small particles easily follow the gas flow. Any local excess of deposited particles would increase the local flow resistance through the wall and force more of the subsequent particle-laden gas through the less-heavily loaded sections, thereby stabilizing the uniform particle loading. Also, since the flow rates down the monolith channels are sufficiently large so that conductive heat transfer between the channel gas and the monolith walls is negligible compared to convective transport in the channels, the entire lengths of the channels will be exposed to similar temperatures. For very low flow rates, as occur when the engine is idling or only part of the exhaust flow is directed through the monolith, further analysis based upon the research presented here can be used to predict variations of the system response along the lengths of the channels (Bissett, 1984).

The conservation of mass can be represented by the following equation:

$$\frac{\partial(\rho v)}{\partial x} = 0 \tag{1}$$

Any reactant mass added to the gas phase from deposit combustion is negligible compared to the convected mass flux. Integrating this equation gives:

$$\rho v = F(t)/A \tag{2}$$

Assuming that the main reaction is a first-order heterogeneous oxidation of carbon and that diffusion is negligible compared to

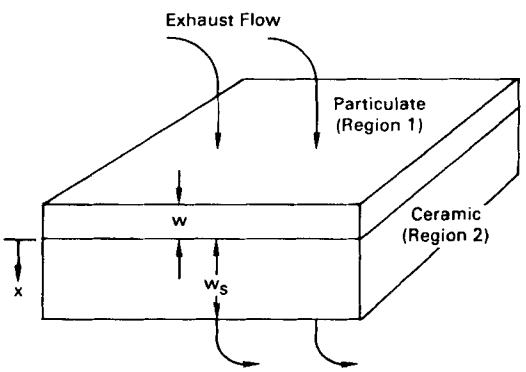

Figure 3. Model geometry for a section of the filtration area of a wall-flow monolith.

convection, the oxygen balance equation is:

$$\frac{\partial}{\partial x}(\rho v y) = -s_j k_j \rho y \quad j = 1,2 \tag{3}$$

where subscript j identifies regions 1 and 2. In introducing y in Eq. 3 it has been assumed that the gas molecular weight is constant. This is a good assumption because the changes in the molar and mass flow rates are negligible. Since there is no reaction in region 2, $k_2 = 0$. The coefficient k_1 for region 1 is calculated from the rate expression suggested by Field et al. (1967) for carbon oxidation.

$$k_1 = kT \exp(-E/RT) \tag{4}$$

Preliminary calculations showed that a typical length scale over which the gas temperature adjusts to differences with the solid temperature is several orders of magnitude smaller than typical deposit layer thicknesses. Therefore it is assumed that the gas and the solid temperatures are equal except at the inlet face of the deposit layer, $x = -w$. It is also assumed that the heat losses to the surroundings are negligible due to proper insulation. Therefore, the heat conservation equation for the solid phase is:

$$\rho_j C_{pj} \frac{\partial T}{\partial t} = s_j(-\Delta H/M_a)k_j \rho y + \frac{\partial}{\partial x}\left(\lambda_j \frac{\partial T}{\partial x}\right) - \rho v C_{pg} \frac{\partial T}{\partial x}, \quad j = 1,2 \tag{5}$$

The rate of shrinkage of the deposit layer is proportional to the rate of oxygen depletion resulting from reaction throughout the deposit layer:

$$\rho_1 \frac{dw}{dt} = (M_c/M_a)[F(t)/A][y(x = 0) - y(x = -w)] \tag{6}$$

Assuming that the gas mixture is ideal,

$$\rho T = M_a p/R \tag{7}$$

The initial conditions are:

$$T(x, t = 0) = T_b \tag{8}$$

$$w(t = 0) = w_b \tag{9}$$

The boundary conditions at $x = -w$ are:

$$y = y_i(t) \tag{10}$$

$$\lambda_1 \frac{\partial T}{\partial x} = \rho v C_{pg}[T - T_i(t)] \tag{11}$$

where $F(t)$, $y_i(t)$ and $T_i(t)$ are the known conditions of the feed gas. At $x = w_s$,

$$\frac{\partial T}{\partial x} = 0 \tag{12}$$

Moreover, at the interface $x = 0$, the variables y and T are continuous and the conductive heat flux, $\lambda_j(\partial T/\partial x)$ is conserved.

METHOD OF SOLUTION

To begin the solution, Eq. 2 is used to eliminate v from the system. Remaining references to ρ are eliminated in favor of T using the equation of state, Eq. 7. The resulting system is then nondimensionalized to yield the following:

For $-\bar{w} < \bar{x} < \bar{w}_s$, $\bar{x} \neq 0$:

$$\bar{F} \frac{\partial y}{\partial \bar{x}} = -\bar{k}_j(\bar{T}) y/\bar{T} \quad j = 1,2 \tag{13}$$

$$\bar{C}_{pj} \frac{\partial \bar{T}}{\partial \bar{t}} = \frac{1}{\epsilon} \frac{\partial}{\partial \bar{x}}\left(\bar{\lambda}_j \frac{\partial \bar{T}}{\partial \bar{x}}\right) + \overline{\Delta H} \bar{k}_j(\bar{T}) y/\bar{T} - \bar{F} \frac{\partial \bar{T}}{\partial \bar{x}} \quad j = 1,2 \tag{14}$$

$$\frac{d\bar{w}}{d\bar{t}} = \overline{M} \bar{F} y|_{-\bar{w}}^{0} \tag{15}$$

For $\bar{x} = -\bar{w}$:

$$y = y_i \tag{16}$$

$$\frac{1}{\epsilon} \frac{\partial \bar{T}}{\partial \bar{x}} = \bar{F}(\bar{T} - \bar{T}_i) \tag{17}$$

For $\bar{x} = \bar{w}_s$:

$$\frac{\partial \bar{T}}{\partial \bar{x}} = 0 \tag{18}$$

At $\bar{t} = 0$, $\bar{T}$ and $\bar{w}$ are 1. Also y, $\bar{T}$, and $\bar{\lambda}_j(\partial \bar{T}/\partial \bar{x})$ are continuous at $\bar{x} = 0$.

The solution is obtained by perturbation expansions of $\bar{T}$, y, and $\bar{w}$ in the small parameter, ϵ. For example,

$$\bar{T} = T_0 + \epsilon T_1 + \epsilon^2 T_2 + \ldots \tag{19}$$

Only the leading order terms will be determined. Although the resulting approximation will differ from the true solution by terms of order ϵ, this is an excellent compromise when considering the exceedingly complex structure of the system. Note especially the nonlocal character of Eq. 15 and the presence of the moving boundary at $\bar{x} = -\bar{w}$. Moreover, since ϵ is estimated to be approximately 9×10^{-4} for the parameter range of interest here, numerical accuracy of this approximation should be excellent. The small size of ϵ, which results from the large solid phase conductivity, and the existence of the moving boundary are both unique properties of this system that are absent in typical fixed-bed reactors.

The leading-order terms of Eqs. 14, 17, and 18 are

$$\frac{\partial}{\partial \bar{x}}\left(\lambda_j \frac{\partial T_0}{\partial \bar{x}}\right) = 0, \quad j = 1,2 \tag{20}$$

$$\frac{\partial T_0}{\partial \bar{x}} = 0 \text{ at } \bar{x} = -w_0, \bar{w}_s \tag{21}$$

The solution of these that is continuous at $\bar{x} = 0$ is

$$T_0 = T_0(\bar{t}). \tag{22}$$

That is, T_0 is uniform in $\bar{x}$, but possesses an as yet unknown dependence on $\bar{t}$.

With this information about T_0, Eq. 13 and its boundary and continuity conditions are readily solved to leading order.

$$y_0 = \begin{cases} y_i \exp\left(-\dfrac{\bar{k}(T_0)}{T_0 \bar{F}}(\bar{x} + w_0)\right) & \bar{x} \leq 0 \\ y_i \exp\left(-\dfrac{\bar{k}(T_0)}{T_0 \bar{F}} w_0\right) & \bar{x} > 0 \end{cases} \tag{23}$$

To determine the behavior of $T_0(\bar{t})$ consider the second-order terms of Eq. 14.

$$\frac{\partial}{\partial \bar{x}}\left(\bar{\lambda}_j \frac{\partial T_1}{\partial \bar{x}}\right) = \bar{C}_{pj} \frac{\partial T_0}{\partial \bar{t}} - \overline{\Delta H} \bar{k}_j(T_0) y_0/T_0 \tag{24}$$

Since T_0 is independent of $\bar{x}$, note that the convective term does not yet appear at this order. After using Eq. 13 at leading order to replace the last term of Eq. 24, it can be integrated from $\bar{x} = -w_0$ to $\bar{w}_s$ to yield the following:

$$\bar{\lambda}_2 \frac{\partial T_1}{\partial \bar{x}}(\bar{w}_s) - \frac{\partial T_1}{\partial \bar{x}}(-w_0) = (\bar{C}_{p1} w_0 + \bar{C}_{p2} \bar{w}_s) \frac{\partial T_0}{\partial \bar{t}} - \overline{\Delta H} \bar{F} y_i \left[1 - \exp\left(-\frac{\bar{k}(T_0) w_0}{T_0 \bar{F}}\right)\right] \tag{25}$$

The boundary terms in this equation are evaluated using the second-order terms of Eqs. 17 and 18.

$$\frac{\partial T_1}{\partial \bar{x}}(\bar{w}_s) = 0 \tag{26}$$

$$\frac{\partial T_1}{\partial \bar{x}}(-w_0) - w_1 \frac{\partial^2 T_0}{\partial \bar{x}^2}(-w_0) = \bar{F}(T_0(-w_0) - \bar{T}_i) \tag{27}$$

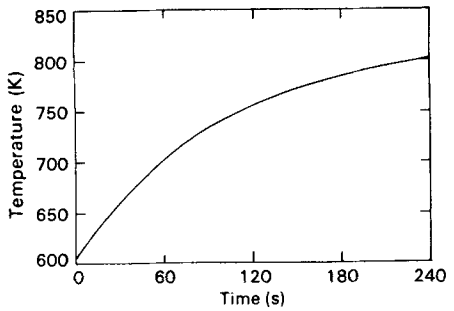

Figure 4. Time dependence of the exhaust gas temperature, T_i, just before it enters the filter.

Recalling that T_0 is independent of $\bar{x}$, substitution of the above two expressions into Eq. 25 gives the dynamic behavior of T_0.

$$\frac{dT_0}{d\bar{t}} = \frac{\bar{F}(\bar{t})}{\bar{C}_{p1}w_0 + \bar{C}_{p2}\bar{w}_s} \cdot \left\{ \overline{\Delta H} y_i(\bar{t}) \left[1 - \exp\left(-\frac{\bar{k}(T_0)w_0}{T_0\bar{F}(\bar{t})} \right) \right] + \bar{T}_i(\bar{t}) - T_0 \right\} \quad (28)$$

Finally, Eq. 15 is written to leading order.

$$\frac{dw_0}{d\bar{t}} = -\overline{M}\bar{F}(\bar{t})y_i(\bar{t}) \left[1 - \exp\left(-\frac{\bar{k}(T_0)w_0}{T_0\bar{F}(\bar{t})} \right) \right] \quad (29)$$

Equations 28 and 29 are readily solved numerically with their initial conditions,

$$T_0(0) = w_0(0) = 1. \quad (30)$$

With T_0 and w_0 thus determined, y_0 is easily obtained at any time from Eq. 23.

Equations 28 and 29 are more than the abstract result of a mathematical manipulation. They could also be obtained directly as overall heat and deposit mass balances, respectively, after assuming oxygen profiles given by Eq. 23 and spatially uniform temperatures, among other assumptions used above.

This singular perturbation procedure is preferred for several reasons. Spatially uniform temperatures are not assumed, they are derived with corrections of order ϵ. The more detailed original problem formulation provides the basis for calculation of these corrections and for quantitatively evaluating the accuracy of these solutions, or for solving the problem for nonuniform initial temperature. Moreover, the above derivation provides a systematic method to justify individually each assumption leading to Eqs. 28 and 29. For example, this approach displays the proper role of the different heat transport processes at the gas-solid interface embodied in Eq. 11 when conductivity is large but the gradients are small.

It should be noted that either if T were not initially independent of x or if the higher-order terms in the solution expansion were desired, then an "inner solution" to the model equations would have to be constructed for the initial time period of order ϵ and asymptotically matched to the "outer solution" calculated above. This analysis will be presented elsewhere (Bissett, 1985).

MODEL PARAMETERS

The parameters describing inlet gas conditions depend on the type of engine and its operating conditions. A typical set of parameters is selected to represent the base condition in the present analysis. The inlet temperature varies with time as shown in Figure 4. Other inlet temperatures are also feasible. However, the important characteristics of the temperature excursion in the filter do not depend significantly on the rate of inlet temperature increase. The mass flow rate, $F(t)$, and the inlet oxygen mole fraction, $y_i(t)$, can be fairly general smooth functions of time in practice and in the application of this model, but are constant for the base condition considered here. The base values for the parameters are

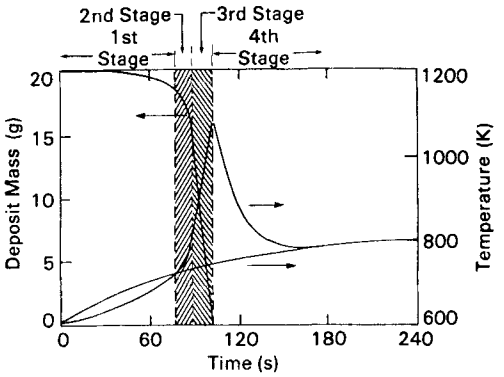

Figure 5. Time dependence of the inlet gas temperature, filter temperature, and deposit mass for the base conditions.

given together with their definitions in the notation section. Monolith properties were obtained from Barin et al. (1977) and Touloukian et al. (1970). The specific area of the deposit layer was calculated from Murphy et al. (1981). w_b is calculated from m by the relation,

$$w_b = m/(\rho_1 A) \quad (31)$$

RESULTS AND DISCUSSION

As discussed earlier, the spatial variation of temperature in the filter is small and has been neglected to the order of accuracy reported in this study. The temporal profiles of filter temperature and particulate mass for regeneration under base conditions are shown in Figure 5. The base values of parameters are given in the notation section. These profiles show that the regeneration process consists of four stages.

The first stage is preheating, during which the filter is slowly responding to the temperature rise of the inlet gas. During this stage the temperature in the filter is lower than the inlet gas and very little reaction takes place.

The second stage begins when reaction starts to become significant and the filter temperature exceeds the inlet temperature. This second stage contains the ignition period of the monolith when the reaction rate increases sharply and the temperature rises steeply.

The third stage begins when the reaction becomes fast enough that nearly all the available oxygen reacts in the deposit layer, and the reaction is limited by the rate of oxygen transport to the deposit. In Eq. 6, $y(x = 0)$ is small compared to $y(x = -w)$ in this stage, as will be discussed shortly. The rate of change of the deposit layer thickness, w, then becomes proportional to the flow rate, $F(t)$, and the incoming oxygen concentration, $y_i(t)$. In the cases considered here where these latter two functions are constants, the time rate of change of w is also constant for this portion of the regeneration as can be seen in Figure 5. In the dimensionless variables, this situation occurs when the exponential in Eqs. 28 and 29 is negligible. If conditions cause the reaction to remain sufficiently weak throughout the regeneration, this stage may not occur.

Finally, the fourth stage is the quenching stage, which starts when the particulate deposit is depleted. During this stage the temperature drops and approaches the inlet gas temperature asymptotically.

The profiles of oxygen concentration across the deposit layer at various times are shown in Figure 6. During the first stage the variation in oxygen concentration is small due to slow reaction. The profiles become increasingly steep during the second stage. Oxygen profiles during the third stage, by definition, have nearly zero values at $x = 0$. During most of the rapid reaction period, the oxygen concentration is small inside most of the particulate layer. Therefore, the reaction occurs mainly in the very thin top layer of deposit. This supports our earlier assumption that during the reaction the thickness of the deposit layer decreases without signif-

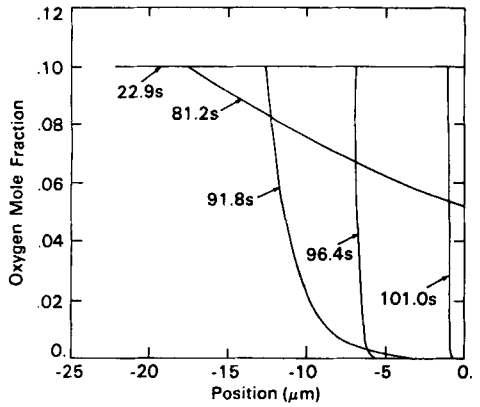

Figure 6. Profiles of oxygen concentration, y, across the deposit layer at selected times. Plots are only drawn between the deposit-substrate interface at position 0 and the deposit surface at $-w$.

icantly affecting the internal structure of the remainder of the layer.

Having discovered these four stages with a fully transient analysis, it is evident that solutions limited to some of the individual stages could be obtained by introducing simplifications, such as selectively neglecting accumulation or reaction, into the model during individual stages. However, such additional efforts can hardly be recommended since the analytical/perturbation analysis described above has already reduced the original system to the straightforward numerical integration of Eqs. 28 and 29 and formula substitution. Even when the solution of Eqs. 28 and 29 is almost steady, stiff integrators solve this system very efficiently.

In addition to clarifying the features of the regeneration process, the model helps to design a suitable system with optimum operating conditions. The most important design requirements within the scope of this study are: (a) long interval between regenerations; (b) short regeneration time; (c) low temperature peak and slow heating and cooling in solid; and (d) small filter size.

To meet these requirements in an optimum design, the effect of various parameters on the regeneration characteristics should be analyzed. As the first step in a systematic parametric study, the

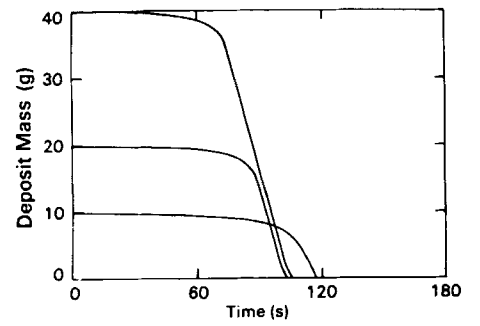

Figure 7a

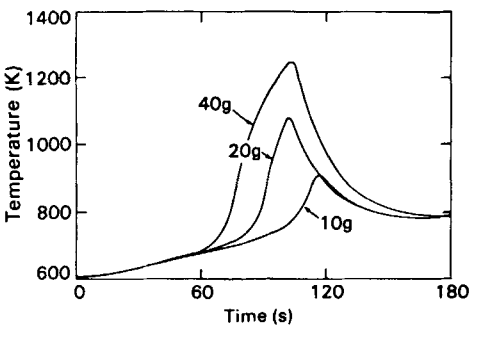

Figure 7b

Figure 7. Effect of variations in initial loading, m.

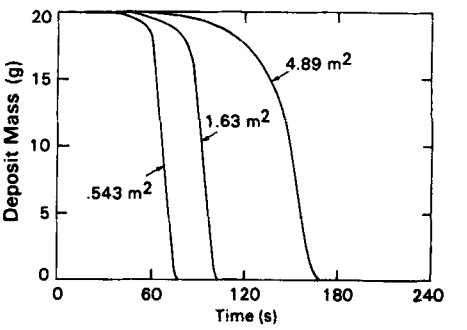

Figure 8a

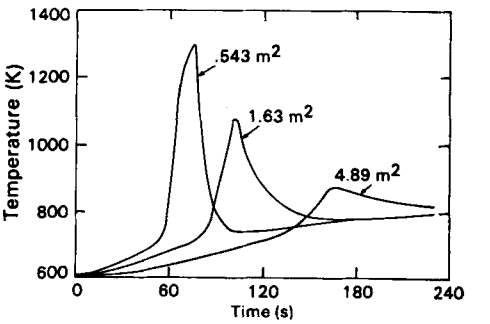

Figure 8b

Figure 8. Effect of variations in filtration area, A.

roles of the most important design variables were investigated for the fixed set of base inlet conditions. The range of variations considered in each case is chosen to be a realistic representative of the range likely to be encountered in practice.

Initial loading is one design variable which can be easily varied by adjusting the frequency of regeneration. High initial loading of particulates is desirable because it allows longer intervals between regenerations. As shown in Figure 7a, the high loading results in a faster ignition with a small change in total regeneration time. The main disadvantage of high loading is the high peak temperature and the rapid excursion of the solid temperature as shown in Figure 7b. The other disadvantage is the higher pressure drop in the filter.

Total filtration area is another important design variable. Filters with smaller areas will be smaller and cheaper. As shown in Figure 8a, the decrease in area with no change in the other parameters speeds up the regeneration process. However, the disadvantage is the steeper and higher solid temperature peaks as shown by Figure 8b. Moreover, the decrease in area increases the pressure drop.

The decrease in area alone affects the regeneration rate by two principal mechanisms. One is by increasing the thickness of the particulate layer, the other is by increasing the gas velocity. The effect of increasing the thickness is the same as that of increasing the initial loading. The effect of increasing the gas velocity is complex; in the range of interest, however, it increases the temperature and reaction rate by bringing more oxygen in contact with the deposit. Therefore, when area is decreased, the above two effects, which are in the same direction, are combined and produce an even larger increase in the rate and the temperature.

Finally, the wall thickness of the filter is another critical design variable. The effects of variations of wall thickness on the regeneration characteristics are shown in Figure 9. A smaller wall thickness gives a faster regeneration but higher and steeper temperature peaks. Changing the channel wall thickness will not affect the filtration efficiency significantly because particles are mainly trapped on the surface and not inside the porous walls (Figure 2). Moreover, a lower wall thickness means a lower pressure drop, which is desirable. Of course, there is a limit on lowering wall thickness which is dictated by the required mechanical strength of the filter and manufacturing limitations.

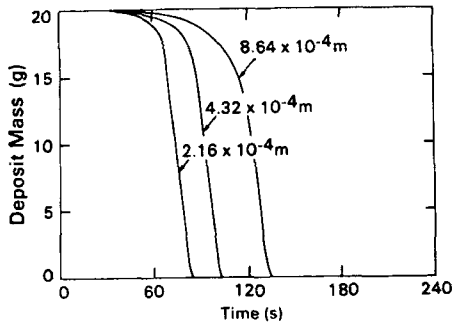

Figure 9a

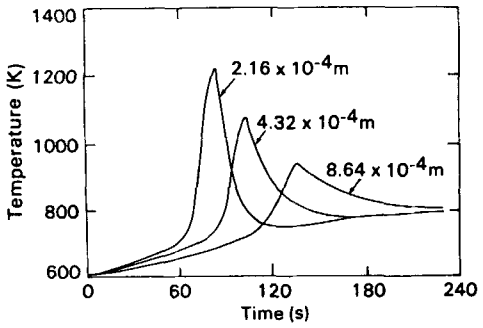

Figure 9b

Figure 9. Effect of variations in wall thickness, w_s.

The results indicate that a good strategy is to choose the thinnest walls allowable for mechanical strength and manufacturing feasibility. The largest filtration area should be chosen within the size limits of the proposed installation. The appropriate loading should be at least great enough to achieve rapid regeneration. In fact, the highest loading that maintains an acceptable pressure drop and keeps the maximum temperature a safe distance under the melting temperature is most desirable because higher loadings increase the capacity of the filter.

The results also show that an acceptable regeneration can be obtained with the parameters selected as the base conditions in this study. This is not the optimum operation; however, the model can be used in conjunction with other design considerations such as mechanical properties, filtration characteristics, and cost to find an optimum design.

ACKNOWLEDGMENT

The authors thank J. S. MacDonald for data on diesel engine exhaust used for the inlet conditions, and G. L. Vaneman and R. Lints for the scanning electron micrograph, Figure 2. All are at General Motors. The authors are also grateful to the reviewers for suggesting several improvements in this paper.

NOTATION

A = filtration area, 1.63 m^2
C_{pg} = heat capacity of gas, 1.09×10^3 J/kg·K
C_{p1} = heat capacity of deposit layer, 1.51×10^3 J/kg·K
C_{p2} = heat capacity of porous ceramic, 1.11×10^3 J/kg·K
$\overline{C}_{pj}$ = dimensionless heat capacity, $C_{pj}\rho_j/(C_{pg}\rho_1)$
E/R = activation energy/gas constant, 1.8×10^4 K
$\overline{F}$ = dimensionless mass flow rate of gas, $F(t)/F(0)$
$F(t)$ = mass flow rate of inlet gas, kg/s
$F(0)$ = initial value of F, 5.23×10^{-2} kg/s
ΔH = heat of reaction, 3.93×10^8 J/kgmol
$\overline{\Delta H}$ = dimensionless heat of reaction, $-\Delta H/(C_{pg}T_bM_a)$
k_j = rate coefficient for the reaction in region j, m/s
k = rate constant defined by Eq. 4, 596 m/s·K
$\overline{k}_j$ = dimensionless rate coefficient, $(s_1 w_b A p M_a k_j)/[RT_bF(0)]$
M_a = molecular weight of gaseous mixture, 29.0 kg/kgmol
M_c = atomic weight of deposit, 12 kg/kgmol
$\overline{M}$ = molecular weight ratio, M_c/M_a
m = initial mass of deposit, 0.02 kg
p = pressure, 101 kPa
R = gas constant, 8.31 m^3·kPa/kgmole·K
s_1 = specific area of deposit layer, 5.5×10^7 m^{-1}
T = temperature, K
$\overline{T}$ = dimensionless temperature, T/T_b
T_b = initial temperature, 606 K
$T_i(t)$ = inlet temperature, K
$\overline{T}_i$ = dimensionless inlet temperature, T_i/T_b
t = time, s
$\overline{t}$ = dimensionless time, $F(0)t/m$
v = superficial velocity, m/s
w = thickness of the particulate deposit layer, m
w_b = initial thickness of the deposit layer, m
$\overline{w}$ = dimensionless deposit thickness, w/w_b
w_s = thickness of wall of monolith channel, 4.32×10^{-4} m
$\overline{w}_s$ = dimensionless wall thickness, w_s/w_b
x = distance, m
$\overline{x}$ = dimensionless distance, x/w_b
y = mole fraction of oxygen
$y_i(t)$ = mole fraction of oxygen at the inlet
$y_i(0)$ = initial mole fraction of oxygen at the inlet, 0.052

Greek Letters

ϵ = dimensionless group $C_{pg}F(0)w_b/A\lambda_1$
λ_1 = bulk thermal conductivity of deposit layer, 0.84 W/m·K
λ_2 = bulk thermal conductivity of porous ceramic, 1.1 W/m·K
$\overline{\lambda}_j$ = ratio of thermal conductivities, λ_j/λ_1
ρ = density of gas, kg/m^3
ρ_1 = bulk density of deposit layer, 5.5×10^2 kg/m^3
ρ_2 = bulk density of porous ceramic, 1.4×10^3 kg/m^3

Subscripts

b = initial condition
i = inlet condition
$j = 1,2$ = indicating region 1 ($j = 1$) and region 2 ($j = 2$)

LITERATURE CITED

Barin, I., O. Knacke, and O. Kubaschewski, *Thermochemical Properties of Inorganic Substances*, 392, Springer-Verlag, Berlin (1977).

Bissett, Edward J., "Mathematical Model of the Thermal Regeneration of a Wall-Flow Monolith Diesel Particulate Filter," *Chem. Eng. Sci.*, 39, 1233 (1984).

———, "Thermal Regeneration of Particle Filters with Large Conduction," *Math. Modeling*, to appear (1985).

Field, M. A., et al., "Combustion of Pulverized Coal," BCURA Leatherhead, 329, Cheroy and Sons, Ltd., Banbury, England (1967).

Johnson, B. M., G. F. Froment, and C. C. Watson, "Temperature Profiles in Packed Beds of Catalyst During Regeneration," *Chem. Eng. Sci.*, **17**, 835 (1962).

Murphy, M. J., L. J. Hillenbrand, and D. A. Trayser, "Assessment of Diesel Particulate Control-Direct and Catalytic Oxidation," SAE Paper 810112 (1981).

Olson, K. E., D. Luss, and N. R. Amundson, "Regeneration of Adiabatic Fixed Beds," *IEC Proc. Des. Dev.*, **7**, 96 (1968).

Rhee, H., D. Fley, and N. R. Amundson, "Creeping Reaction Zone in a Catalytic Fixed-Bed Reactor. A Cell Model Approach," *Chem. Eng. Sci.*, **28**, 607 (1973).

Rhee, H., R. P. Lewis, and N. R. Amundson, "Creeping Profiles in Catalytic Fixed-Bed Reactors. Continuous Models," *IEC Fund.*, **13**, 317 (1974).

Shadman, F., and E. J. Bissett, "Thermal Regeneration of Diesel Particulate Filters: Development of a Mathematical Model," *IEC Proc. Des. Dev.*, **22**, 203 (1983).

Touloukian, Y. S., et al., *Thermal Conductivity, Nonmetallic Solids*, 918, IFI/Plenum, New York (1970).

Manuscript received Feb. 28, 1983; and accepted June 3, 1984.